



# Interannual variations in spring lightning activity and convective rainfall over South China during the TRMM era

Jiangyu Mao<sup>1,2</sup> • Majun Li<sup>1,2</sup>

Received: 6 February 2020 / Accepted: 8 July 2020 / Published online: 21 July 2020  
© Springer-Verlag GmbH Austria, part of Springer Nature 2020

## Abstract

The interannual variability of spring lightning activity over South China (SC) and its driving mechanism are examined using the Tropical Rainfall Measuring Mission (TRMM) satellite-estimated convective rain rate and merged lightning flash rate datasets together with atmospheric and oceanic reanalysis products over the TRMM period (1998–2014). SC is climatologically characterized by high lightning flash densities, strong convective rainfall, and large convective available potential energy (CAPE) during spring. The spring SC lightning activity (SCLA) has a strong year-to-year variability, and the standard deviation of flash rates shows a spatially coherent annular distribution centered over the Pearl River Delta. The interannual variations of spring SCLA are not only highly correlated with those of convective rainfall and CAPE, but also significantly correlated with El Niño–Southern Oscillation (ENSO). The anomalously frequent SCLA tends to follow El Niño events, while infrequent SCLA preferentially follows La Niña events. Composite analyses demonstrate that during spring for the more frequent SCLA cases, the upper tropospheric atmospheric response to El Niño-related sea surface temperature anomaly (SSTA) patterns leads to strong southwesterlies over SC in conjunction with tropical westerlies over the tropical Indian Ocean, forming a divergent environment over SC. The upper-level divergence is coupled with low-level moisture convergence, generating strong mid-tropospheric updrafts to lift more air parcels to reach their level of free convection, thereby producing stronger convection with frequent SCLA. In contrast, the anomalous circulation forced by La Niña-related SSTA patterns is conducive to suppressed convection over SC and infrequent SCLA.

## 1 Introduction

Thunderstorms are a type of locally severe convective weather that is generally produced by cumulonimbus clouds and always accompanied by lightning with strong gusts of wind, heavy rainfall, and sometimes hail (Williams et al. 2000; Zipser et al. 2006). Thunderstorms can significantly disrupt socioeconomic development (Zhang et al. 2011; Dowdy and Mills 2012), and lightning strikes can directly result in loss of life, damage to infrastructure, and wildfires, especially over densely populated and economically developed regions (Holle 2008; Zhang et al. 2011; Dowdy 2016). Therefore, investigating the temporal variation and related mechanisms

of regional lightning activity together with convective rainfall is of great importance for better lightning protection to efficiently prevent and reduce natural disasters.

With the development of satellite-based lightning detection techniques in recent decades, lightning flash rates can be detected globally (Christian et al. 2003; Cecil et al. 2014, 2015). In the global climatology, the annualized (annual rates of) lightning flashes tend to peak over land areas, but vary geographically (Christian et al. 2003; Cecil et al. 2014). Maximum lightning densities occur in coastal areas away from the equator (e.g., North America, eastern Argentina, the Indochina Peninsula, and southeastern China) and mountainous regions (e.g., the Himalayas in northern Pakistan and the Andes of northern Colombia) as these regions are subject to migrating synoptic-scale cyclones, topographic lifting, and monsoonal winds (Petersen et al. 2002; Xu et al. 2009; Ramesh Kumar and Kamra 2012). High lightning densities are also present year-round in the equatorial Congo Basin and Indonesian Archipelago due to intense convective systems within the Intertropical Convergence Zone having larger convective available potential energy (CAPE) over equatorial

✉ Jiangyu Mao  
m jy@lasg.iap.ac.cn

<sup>1</sup> LASG, Institute of Atmospheric Physics, Chinese Academy of Sciences, Beijing 100029, China

<sup>2</sup> University of Chinese Academy of Sciences, Beijing 100049, China

Africa (Monkam 2002) and the western Pacific (Blakeslee et al. 2014). Because the annually averaged global distribution of lightning activity depends strongly on the seasonal evolution of regional flash rates (Christian et al. 2003), the maximum annualized lightning densities are mostly dominated by the lightning activity in the local summer season.

However, for some regions such as the Amazon basin, the most frequent lightning activity occurs during the Southern Hemisphere spring season, because synoptic-scale frontal systems migrate northward into the basin, triggering deeper storms with stronger vertical velocities (Petersen et al. 2002). As shown in Christian et al. (2003) and Blakeslee et al. (2014), a similar situation arises during the Northern Hemisphere spring season (March–May), with more frequent lightning activity of greater than  $2 \times 10^{-2}$  fl km<sup>-2</sup> day<sup>-1</sup> over South China (SC; specifically south of 30° N around the Yangtze Basin). Such lightning densities have comparable magnitude to those during the summer season (June–August), indicating that spring is another dominant period to produce frequent lightning for SC. These characteristics are supported by Dai et al. (2009), who pointed out that convective weather varies with region and season in China; with the pre-monsoon beginning in SC in April and May, lightning associated with thunderstorms increases in frequency. In fact, such lightning-related heavy rains climatologically start near mid-March, forming a heavy rain-belt that remains over SC for the entire spring season (LinHo et al. 2008). Subsequently, the heavy rain-belt migrates to the Yangtze Basin around mid-June and then reaches North China by late July (Tao and Chen 1987). Since the SC spring rainfall is characterized by the first rainy episode after the dry winter season, it is of interest to examine why there is so much lightning in SC during spring.

Atmospheric instability, ambient moisture, wind shear, and other lifting factors are crucial to thunderstorms and lightning (Dai et al. 2009), so some studies have examined the physical relationship of lightning occurrence with convective rainfall and instability indices such as CAPE (Yuan and Qie 2008; Xu et al. 2010; Cecil et al. 2015; Zheng et al. 2016). In southeastern China, Dai et al. (2009) found a close dependence of lightning activity on some convective indices (e.g., CAPE, lifted condensation level) over SC for the spring and summer seasons. Zheng et al. (2016) again suggested that spring lightning activity over SC is more sensitive to CAPE than that over offshore waters. Therefore, it is useful to explore how the spring total lightning activity and related convective indices over SC vary on interannual timescales.

Given that the El Niño–Southern Oscillation (ENSO) phenomenon is a dominant interannual variability in the ocean–atmosphere system, it affects significantly the tropical, subtropical, and mid-latitude climate, leading to persistent temperature and precipitation anomalies in many regions during winter and following spring (Wang et al. 2000; Feng and Li 2011; Wu and Mao 2016, 2018). Wang et al. (2000) suggested that El Niño

(La Niña) events tend to induce an anomalous lower tropospheric anticyclone (cyclone) locating in the western North Pacific during winter, and such anticyclonic (cyclonic) anomalies persist until the following spring or early summer, causing anomalously wet (dry) conditions over eastern China extending from SC northeastward to the east of Japan. Further, the influence on spring rainfall over SC of the central Pacific-type El Niño event was even found to differ from that of typical eastern Pacific-type El Niño events (Feng and Li 2011). With regard to possible impacts of ENSO events on lightning activity, they have been explored by some previous studies for various regions (e.g., Goodman et al. 2000; Yoshida et al. 2007; Chronis et al. 2008; Dowdy 2016; Saha et al. 2017). Using 6 years of data from 1998 to 2003 that included two El Niño and one La Niña events, Yoshida et al. (2007) found that the annual lightning flash rate increases (decreases) during El Niño (La Niña) periods in East/Southeast Asia, especially over SC. Subsequently, Chronis et al. (2008) utilized the same 6-year dataset to calculate simultaneous temporal correlations between the monthly Niño 3.4 index time series and the monthly lightning flash rate anomaly time series for every grid point. They identified that significant positive correlations occur over southeastern China, the southern Mediterranean, and North Africa while significant negative correlations occur over northern Australia and northeastern South America. Comparing more ENSO cases, Yuan et al. (2016) noted that the areas of positive (negative) lightning anomalies are located mainly on both sides of 5°–20° N (5°–15° N) in El Niño (La Niña) boreal spring and winter, but north of the equator in summer and autumn. Dowdy (2016) again emphasized that ENSO has a strong relationship with lightning activity during each individual season by calculating the simultaneous correlations of seasonal lightning activity over the global tropical and temperate regions with the Niño 3.4 index. He found that the most significant positive correlations between lightning activity and ENSO over SC occur during spring. These studies suggest that the seasonal lightning activity over SC may be affected by ENSO events, but these results are either only based on simultaneous monthly and seasonal correlations rather than time-lagged correlations or simply based on composites for a few ENSO cases without any test of statistical significance for lightning anomalies. Thus, it is necessary to examine how wintertime ENSO affects lightning activity in the following season over SC using multi-year lightning data, because the ENSO-induced atmospheric circulation anomaly pattern tends to persist for several months (Wang et al. 2000; Wu and Mao 2016).

The spring rainy season over SC is the first stage of the seasonal northward shift of the heavy rain-belt for China, with SC being characterized by higher lightning densities during spring. Given that the lightning occurrence depends on the large-scale atmospheric circulation condition favorable to mesoscale convective systems, and ENSO is a dominant external

forcing to generate significant interannual fluctuations of the atmospheric circulation over the East Asian region, the objective of this study is to reveal the interannual variability of spring SC lightning activity (hereafter SCLA) in relation to convective rainfall and CAPE, exploring the physical mechanisms of how anomalous large-scale circulations associated with sea surface temperature (SST) anomalies (SSTAs) cause anomalously frequent and infrequent SCLA.

## 2 Data and methods

### 2.1 Data

The monthly lightning flash rate data used in this study are gridded flash products ( $2.5^\circ \times 2.5^\circ$  resolution bins), which are extracted from the Low Resolution Monthly Climatology Time Series (LRMTS) data file (LRMTS\_COM\_FR, as described in Cecil et al. 2014) archived at the Global Hydrology Resource Center for the period 1998–2014. The LRMTS lightning flash rates were actually detected by two lightning detection sensors, the spaceborne Optical Transient Detector (OTD) on the MicroLab-1 satellite (available for the period May 1995–March 2000) and the Lightning Imaging Sensor (LIS) onboard the Tropical Rainfall Measuring Mission (TRMM) satellite launched in November 1997, with flash counts from each instrument being scaled by the best available estimates of detection efficiency (Christian et al. 2003). As such, both OTD-detected and LIS-detected flash rates as well as the merged LIS/OTD flash records are available to examine the spatial and temporal variations of lightning activity (Cecil et al. 2014, 2015).

Note that the merged LIS/OTD lightning flash products utilized in the present study were only available till December 2014 because TRMM satellite was removed from orbit in April 2015. Actually, the merged LIS/OTD flash rate for each grid box was calculated as the weighted average of the low resolution time series of the smoothed daily flash rates from LIS and OTD (Cecil et al. 2014). Note that considerable spatial and temporal smoothing were applied to obtain the individual time series of the smoothed daily flash rates for LIS and OTD, using a  $7.5^\circ \times 7.5^\circ$  boxcar moving average and a 111-day boxcar moving average on the flash counts and viewtimes. A detailed description of the computational procedure and detailed evaluation of such combined LIS/OTD LRMTS flash rate data may be found in Cecil et al. (2014).

Monthly rain rates for total rainfall and its convective and stratiform components were derived from the TRMM 3A25v7 product at  $0.5^\circ \times 0.5^\circ$  horizontal resolution. These data have been used to examine the multi-scale variability of convective and stratiform rainfall in the Asian monsoon regime (e.g., Li et al. 2009; Pokhrel and Sikka 2013). The TRMM satellite-estimated convective rain rate and lightning flash rate

products currently include data for more than 17 years. Thus, these products can be used to investigate the interannual variation of convective rainfall and consequent lightning activity.

To investigate the atmospheric circulation conditions responsible for the interannual variability in spring SCLA, monthly meteorological variables and parameters such as horizontal winds at various isobaric surfaces and CAPE are taken from the European Centre for Medium-Range Weather Forecasts (ECMWF) ERA-Interim datasets (Berrisford et al. 2009; Dee et al. 2011), with a resolution of  $0.75^\circ \times 0.75^\circ$  from 1998 to 2014. Note that as a thermodynamical parameter to represent potential buoyancy available to idealized rising air parcels, CAPE is an instantaneous variable similar to lightning. However, its daily and monthly mean values can still signify the local instability situation of the tropospheric atmosphere for the corresponding timescales (Williams and Renno 1993; Dai et al. 2009; Zheng et al. 2016). The ERA-Interim reanalysis system thus produces directly the monthly CAPE outputs, and such monthly CAPE data are commonly used to demonstrate the seasonal changes of CAPE globally or regionally in relation to the occurrence of extreme weather events such as thunderstorms (Trapp et al. 2007; Dai et al. 2009; Zheng et al. 2016). Note that the high-resolution products of convective rain rates are interpolated onto the same  $0.75^\circ \times 0.75^\circ$  grid to match CAPE data.

Monthly SST data are from the newly updated Extended Reconstructed SST (ERSST) product (ERSSTv5; Huang et al. 2017) on a  $2^\circ \times 2^\circ$  grid from the National Oceanic and Atmospheric Administration (NOAA). The corresponding Oceanic Niño Index (ONI) is thus used to characterize warm or cold ENSO events, and it is downloaded directly from the website of the NOAA Climate Prediction Center. Note that the ONI is calculated as the 3-month running mean of ERSSTv5 SST anomalies in the Niño 3.4 region ( $5^\circ\text{S}$ – $5^\circ\text{N}$  and  $120^\circ$ – $170^\circ\text{W}$ ), with an El Niño (La Niña) event being typically identified when the ONI is greater (less) than  $0.5^\circ\text{C}$  ( $-0.5^\circ\text{C}$ ) for a minimum of five consecutive overlapping seasons. Note also that although the ONI is very similar to the most widely used Niño 3.4 index, the SST anomalies in the ONI definition are averaged over a shorter period and require shorter longevity and a higher anomaly threshold than the Niño 3.4 index.

### 2.2 Key area and regional SCLA index

The topography of the southern part of China is shown in Fig. 1a; the longitude of  $105^\circ\text{E}$  is usually considered as the eastern boundary of the Tibetan Plateau that is mostly above 1500 m (Wan and Wu 2007); the region farther east has lower altitude. Note that besides the foothills on the eastern slopes of the Tibetan Plateau with topography above 500 m, there are two larger mountain ranges within SC. One is the Nanling

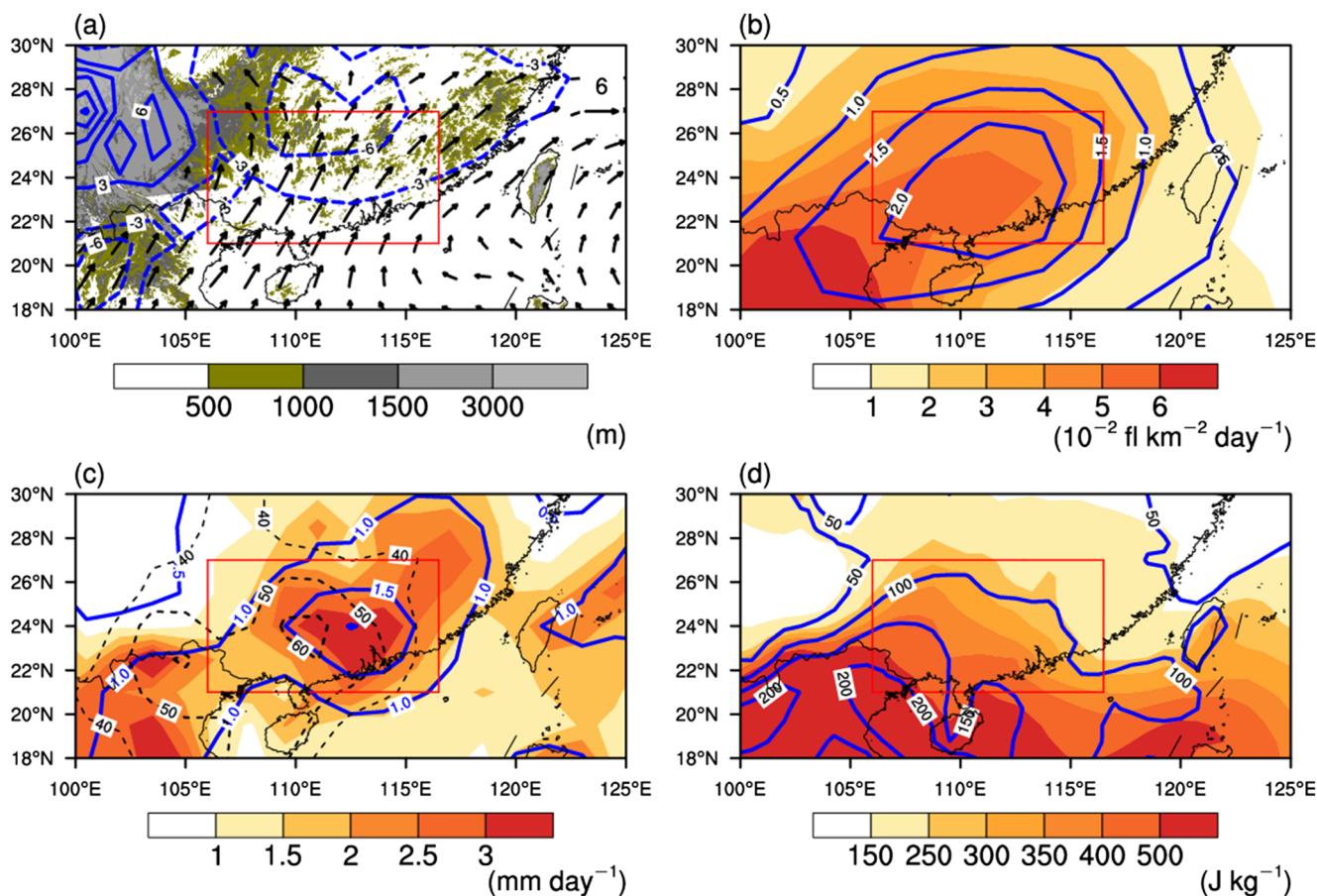


**Fig. 1** Spatial distributions of **a** topography (shading; m) along with climatological spring (March–May) 850-hPa winds (vectors;  $\text{m s}^{-1}$ ) and 500-hPa vertical velocity (blue contours, dashed where negative;  $10^{-2} \text{ Pa s}^{-1}$ ), **b** climatology (shading) and standard deviations (blue contours) of spring lightning flash rate (FR,  $10^{-2} \text{ fl km}^{-2} \text{ day}^{-1}$ ), **c** as in **b** except for spring convective rainfall rate (ConvR;  $\text{mm day}^{-1}$ ), and **d** as in

**b** except for spring convective available potential energy (CAPE;  $\text{J kg}^{-1}$ ) for the period 1998–2014. Note that the black dashed contours in **c** denote the interannual standard deviation of convective rainfall as a percentage (%) of total (convective plus stratiform) rainfall. The red rectangle indicates the key region over South China ( $21^{\circ}$ – $27^{\circ}$  N,  $106^{\circ}$ – $116.5^{\circ}$  E)

mountains (east–west oriented hills,  $24^{\circ}$ – $26.5^{\circ}$  N,  $110^{\circ}$ – $116^{\circ}$  E, with terrain heights of 500–1000 m), and the other is the Wuyi mountains (northeast–southwest orientated hills,  $25^{\circ}$ – $29^{\circ}$  N,  $116^{\circ}$ – $119^{\circ}$  E, with an average height of  $\sim 1000$  m) (Wan and Wu 2007; LinHo et al. 2008). Climatologically, strong southwesterly winds prevail in the lower troposphere over SC during spring (Fig. 1a), with strong ascending motion of magnitude greater than  $3 \times 10^{-2} \text{ Pa s}^{-1}$  in the middle troposphere, leading to spring total (convective plus stratiform) rainfall greater than 400 mm, as shown in Wu and Mao (2016). Note that the Nanling mountains act as a physical barrier to the southwesterlies as the wind direction is almost perpendicular to the zonal mountain range. Air parcels are inevitably lifted over the mountains, especially over the windward side, producing strong cumulonimbus clouds and convective rainfall (Fig. 1c). The climatological distribution derived from the merged LIS/OTD lightning flash rate data for the period 1998–2014 shows a high frequency of lightning activity (greater than  $2 \times 10^{-2} \text{ fl km}^{-2} \text{ day}^{-1}$ ) over SC (Fig.

1b), with maximum lightning flash densities (greater than  $5 \times 10^{-2} \text{ fl km}^{-2} \text{ day}^{-1}$ ) concentrated over Guangxi Zhuang Autonomous Region and Guangdong province, consistent with the results from ground-based lightning detection systems (Zheng et al. 2016).

The area with maximum flash density above  $5 \times 10^{-2} \text{ fl km}^{-2} \text{ day}^{-1}$  mostly comprises two coastal regions [the Pearl River Delta (PRD) and western Guangdong Province including a southeastern portion of Guangxi Zhuang Autonomous Region] as classified by Dai et al. (2009), who compared LIS-detected lightning flash rates with several convective indices for a number of regions in China. Figure 1b also displays the interannual standard deviation of the spring lightning flash rate over SC based on data from 1998 to 2014, with magnitude mostly exceeding  $1.0 \times 10^{-2} \text{ fl km}^{-2} \text{ day}^{-1}$ , indicating an evident year-to-year variability. The interannual standard deviations are spatially coherent over SC, with an annular distribution centered over western Guangdong Province (Fig. 1b). Note that the area

encircled by the innermost closed isoline of standard deviation equal to  $2.0 \times 10^{-2} \text{ fl km}^{-2} \text{ day}^{-1}$  just corresponds to the domain of maximum climatological flash density over SC, but the locations with even larger climatological flash densities over the northeastern Indochina Peninsula exhibit weaker interannual variability.

To investigate the interannual variability of the SCLA, a key area has to be selected to define an index to represent regional lightning flash rate. As shown in Fig. 1b, the closed isoline of the standard deviation equal to  $1.5 \times 10^{-2} \text{ fl km}^{-2} \text{ day}^{-1}$  roughly covers most of the regions with climatological flash densities equal to or greater than  $3.0 \times 10^{-2} \text{ fl km}^{-2} \text{ day}^{-1}$  over SC. This is equivalent to the amplitude of interannual fluctuations reaching half of the local climatological flash densities. Therefore, we use the standard deviation of  $1.5 \times 10^{-2} \text{ fl km}^{-2} \text{ day}^{-1}$  as a threshold to define the key area ( $21^{\circ}$ – $27^{\circ}$  N,  $106^{\circ}$ – $116.5^{\circ}$  E; the red rectangle in Fig. 1b). Thus, the area-averaged spring lightning flash rate over this key area is defined as the regional SCLA index. The time series of area-averaged SCLA anomalies is computed over the key area from 1998 to 2014 (Fig. 2). Note that the anomalies refer to the departures from the long-term mean for the period 1998–2014, and the long-term mean is  $4.5 \times 10^{-2} \text{ fl km}^{-2} \text{ day}^{-1}$ . The interannual standard deviation (indicated by  $\sigma$ ) for this period is  $1.76 \times 10^{-2} \text{ fl km}^{-2} \text{ day}^{-1}$ . Considering that the interannual standard deviations of lightning activity are spatially coherent over SC, and the isoline of the threshold encloses most of SC (Fig. 1b), this relatively large key area can represent well the regional behavior of spring lightning activity over the entire SC. This key area is slightly larger than that defined by Dowdy (2016), who selected a region of  $7.5^{\circ} \times 7.5^{\circ}$  mostly covering Guangxi and Guangdong provinces to demonstrate the simultaneously strong correlation between SCLA and ENSO in spring. Note that the

maximum flash densities especially within the key area (Fig. 1b) correspond to locations with maximum convective rainfall and CAPE (Fig. 1c, d), so the spatial and interannual variability of spring SCLA in relation to convective rainfall and CAPE in the same season will be discussed in Section 3.1.

### 2.3 Classification of anomalous SCLA years and composite analysis

Using the SCLA anomaly time series for the period 1998–2014 (Fig. 2), linear correlation is applied to examine the relationships of SCLA with local atmospheric instability parameters such as CAPE and remote forcing such as ENSO. Pearson correlation coefficients are thus calculated between time series of area-averaged spring lightning flash rate and other variables such as convective rainfall and SST. The statistical significance of linear correlations is tested based on two-tailed probabilities (Li and Mao 2019).

Composite analyses are applied to anomalously high versus anomalously low SCLA years to examine the physical mechanisms responsible for the interannual variability of regional lightning activity over SC in spring. As shown in Fig. 2, the time series of SCLA anomalies exhibits evident interannual fluctuations with different amplitudes. For example, positive anomalies in 1998 and 2013 considerably exceed  $1.76 \times 10^{-2} \text{ fl km}^{-2} \text{ day}^{-1}$  (one standard deviation,  $+1\sigma$ ), suggesting that these are anomalously high SCLA years. The opposite situation is found in anomalously low SCLA years such as 1999 and 2011, with negative anomalies being much less than  $-1\sigma$ . As such, years can be categorized as having anomalously high and low SCLA based on  $1\sigma$  as a threshold. However, given that statistically reliable composite results are derived from large samples, and assuming that the SCLA time series follows a normal distribution with an equal number of

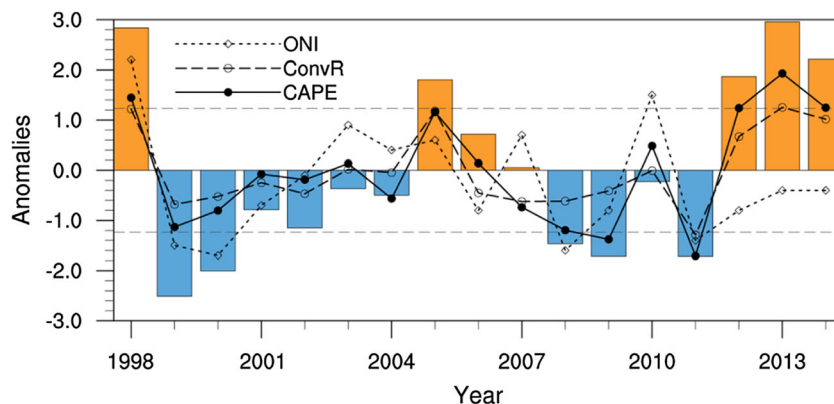


**Fig. 2** Time series of area-averaged spring (March–May) lightning flash rate (bar;  $10^{-2} \text{ fl km}^{-2} \text{ day}^{-1}$ ), convective rainfall rate (long dashed curve;  $\text{mm day}^{-1}$ ), and CAPE (solid curve;  $\text{J kg}^{-1}$ ) anomalies over the SC key region ( $21^{\circ}$ – $27^{\circ}$  N,  $106^{\circ}$ – $116.5^{\circ}$  E) from 1998 to 2014, with anomalies calculated as departures from the 1998–2014 climatology for each variable. Also shown is the time series of area-averaged winter (December–

February) Oceanic Niño Index (ONI) (short dashed curve;  $^{\circ}\text{C}$ ) over the Niño 3.4 region ( $5^{\circ}$  S– $5^{\circ}$  N,  $120^{\circ}$ – $170^{\circ}$  W). Parallel dashed lines indicate 0.7 times the standard deviation of the time series of area-averaged lightning flash rate anomalies used as the threshold to categorize anomalously frequent and infrequent SCLA years

amplitudes above and below the mean value, the threshold is reduced to  $0.7\sigma$  to extract relatively more samples for composite analysis. Thus, years with anomalously high (low) SCLA are defined as having an amplitude of lightning flash rate anomaly greater (less) than  $0.7\sigma$  ( $-0.7\sigma$ ), and these are termed frequent (infrequent) SLCA years. This classification not only assures that departures of the selected anomalous lightning years exceed half of a standard deviation, but also produces a reasonable separation with five frequent SCLA years (1998, 2005, 2012, 2013, and 2014) and five infrequent SCLA years (1999, 2000, 2008, 2009, and 2011). The composite analyses are produced for these frequent and infrequent SCLA years in terms of convective rainfall, CAPE, horizontal winds on different isobaric surfaces, and SST, with the statistical significance of the composite anomalies being assessed using Student's *t* test.

### 3 Results

#### 3.1 Climatological features

As mentioned in Section 2.2, the spring rainy season over SC is climatologically dominated by lower tropospheric southwesterlies (Fig. 1a). Because such prevailing southwesterlies are associated not only with the western North Pacific subtropical anticyclone but also with the upstream veered flow around the Tibetan Plateau related to both mechanical and thermal forcing (Wan and Wu 2007), they favor the formation of synoptic-scale quasi-stationary frontal systems when they encounter the equatorward-intruding cold air over SC (LinHo et al. 2008). In turn, some mesoscale convective systems associated with the cold or warm frontal systems are triggered by the Nanling and Wuyi mountains (LinHo et al. 2008; Xu et al. 2009; Yuan et al. 2016; Zheng et al. 2016), leading to strong ascending motion in the middle troposphere (Fig. 1a), thereby producing intense thunderstorms with more lightning flashes (Fig. 1b) and resultant convective rainfall (Fig. 1c). Note in Fig. 1b that within the key area the isoline of  $5 \times 10^{-2}$  fl km<sup>-2</sup> day<sup>-1</sup>, which represents the northern boundary of the innermost sub-region having maximum flash densities, is roughly parallel to the Nanling mountains (Fig. 1a). The lightning densities decrease northward toward the Yangtze Basin (Fig. 1b). TRMM satellite-estimated convective rainfall is indeed dominant over SC, with the rainfall rates being mostly greater than  $1.5$  mm day<sup>-1</sup> (Fig. 1c). Note that a sub-region with maximum rainfall rates exceeding  $3$  mm day<sup>-1</sup> is present around the PRD near Guangzhou City, corresponding well to the area of maximum flash densities (Fig. 1b). The convective rainfall (Fig. 1c) accounts for 55% of the spring total (convective and stratiform) rainfall shown in Wu and Mao (2016) over most of SC, with an even larger proportion (>65%) occurring over the PRD, indicating that convective rainfall dominates

stratiform rainfall in this region. Note that convective rainfall (Fig. 1c) exhibits a similar spatial distribution to lightning density (Fig. 1b), with the isoline of  $2.5$  mm day<sup>-1</sup> coinciding with the Nanling mountains (Fig. 1a). Another strong convective rain-belt ( $>2.5$  mm day<sup>-1</sup>; Fig. 1c) is present along the Wuyi mountains (Fig. 1a), corresponding to the frequent lightning activity that is characterized by the northeastward protruding isolines of flash density (Fig. 1b). These features demonstrate the role of both synoptic-scale circulation forcing and topographic lifting in triggering thunderstorms. This is partly supported by the strong ascending motion shown in Fig. 1a, because such ascending motion is involved in both convective and stratiform rainfall. As suggested by Williams (1995), the topographic lifting of air parcels in mountain areas is related to CAPE, because it can provide the finite vertical displacement to initiate conditional instability and provide the CAPE required for the formation of thunderstorms. The climatological CAPE in spring (Fig. 1d) also has a similar spatial distribution to lightning flash density over SC (Fig. 1b), with larger CAPE ( $>400$  J kg<sup>-1</sup>) decreasing northward to  $150$  J kg<sup>-1</sup> around the Yangtze Basin (Fig. 1d). Along the Nanling mountains, the CAPE values range from 300 to  $400$  J kg<sup>-1</sup>, indicating that the larger lightning densities and convective rainfall around the Nanling mountains are indeed associated with larger CAPE. Although CAPE is lower ( $150$  J kg<sup>-1</sup>) along the Wuyi mountains (Fig. 1d), topographic lifting is still the important mechanism that causes such an unstable air mass to rise and produce strong convective rainfall along with lightning flashes (Fig. 1b, c). The close dependence of lightning activity on CAPE over SC is further supported by Zheng et al. (2016), who noted that in the climatology and over the southern portion of the key area with largest flash densities, the monthly variations of lightning density increase linearly with CAPE from March until they reach a peak in May.

#### 3.2 Interannual variation

The spatial distributions of the interannual standard deviations of spring lightning activity, convective rainfall, and CAPE are shown in Fig. 1b–d, respectively, for 17 years of data from 1998 to 2014. As mentioned in Section 2.2, the standard deviations of the spring lightning activity are characterized by a spatially coherent annular distribution, with maxima greater than  $3.0 \times 10^{-2}$  fl km<sup>-2</sup> day<sup>-1</sup> concentrated around the PRD (Fig. 1b). Convective rainfall rates also have considerable interannual variability, with standard deviation mostly greater than  $1.0$  mm day<sup>-1</sup> over SC (Fig. 1c) and showing a similar coherent distribution to that of the lightning flash rates (Fig. 1b). Note that such interannual variability of convective rainfall reflects to a great extent that of total (convective plus stratiform) rainfall, because the interannual standard deviations of convective rainfall are mostly greater than 50% of those of total rainfall, even above 60% over Guangxi and

Guangdong provinces (Fig. 1c). This implies that convective rainfall variability associated with lightning activity makes a major contribution to regional climate variation over SC. Note also that the maximum standard deviations for both convective rainfall rates and lightning flash rates are all located around the PRD (Fig. 1b, c). Similarly, CAPE exhibits an evident interannual fluctuation (Fig. 1d). Although the spatial distribution of the standard deviation of CAPE is relatively less coherent and the maximum standard deviations are not located over the PRD, the standard deviation of CAPE is mostly on the order of 100–150 J kg<sup>-1</sup> over the key area (Fig. 1d). Such large standard deviations of CAPE correspond to those of lightning flash rates and convective rainfall rates, indicating a close connection between lightning activity, convective rainfall, and CAPE on interannual timescales.

To further examine the connection of SCLA with other variables on interannual timescales, Fig. 2 displays time series of area-averaged spring convective rainfall and CAPE anomalies over the SC key region from 1998 to 2014. The spring convective rainfall rate and CAPE indeed exhibit similar year-to-year fluctuations to SCLA although with larger amplitudes, and they are highly correlated. Note in Table 1 that the correlation coefficient between the time series of SCLA and convective rainfall anomalies is 0.92, which is statistically significant at the 99% confidence level, indicating that the variation of lightning activity is consistent with that of convective intensity, as suggested by Zipser et al. (2006). Similarly, the area-averaged CAPE also has highly significant correlations with SCLA and with convective rainfall, with the correlation coefficients reaching 0.93 and 0.95, respectively (Table 1). Such a strong correlation between SCLA and CAPE over SC is consistent with that reported by Dowdy (2016), who suggested that a CAPE-related thermodynamic environment seems to play a significant role in producing deep convection and resultant lightning. These results indicate that the spring SCLA and convective rainfall are indeed strongly dependent on CAPE on interannual timescales, and more frequent SCLA and stronger convective rainfall are associated with larger CAPE over SC.

**Table 1** Pearson correlation coefficients between time series of area-averaged anomalies over the SC key region (21°–27° N, 106°–116.5° E) in terms of spring lightning flash rate (FR; 10<sup>-2</sup> fl km<sup>-2</sup> day<sup>-1</sup>), convective rainfall rate (ConvR; mm day<sup>-1</sup>), convective available potential energy (CAPE; J kg<sup>-1</sup>), and time series of wintertime ONI (°C) for the period 1998–2014. The coefficients in italics (boldface) are statistically significant at the 95% (99%) confidence level

	FR	ConvR	CAPE	ONI
FR	1	<b>0.92</b>	<b>0.93</b>	<i>0.51</i>
ConvR		1	<b>0.95</b>	<i>0.51</i>
CAPE			1	<i>0.51</i>
ONI				1

To demonstrate the spatial coherence of the anomalous SCLA over SC, in association with the anomalous convective rainfall and CAPE, Fig. 3 shows the composite anomalies for the frequent versus infrequent SCLA years and their differences in terms of lightning flash rate, convective rainfall, and CAPE. Significant positive anomalies of lightning flash rate are present over SC during the frequent SCLA years (Fig. 3a), with anomaly maxima above  $3 \times 10^{-2}$  fl km<sup>-2</sup> day<sup>-1</sup> concentrated around and south of the Nanling Mountains and accompanied by significant positive anomalies of convective rainfall (Fig. 3d). Although CAPE maxima are located over the southwest corner of SC, positive CAPE anomalies are still statistically significant over the entire SC (Fig. 3g). The opposite situations occur during the infrequent SCLA years (Fig. 3b, e, and h). An apparent exception is noted in convective rainfall (Fig. 3e), with statistically significant negative anomalies over a much wider region especially north of the Nanling mountains, which may be an asymmetric response to external forcing of La Niña events (as discussed below). The composite differences between frequent and infrequent SCLA years show similar patterns to those in the frequent SCLA years. Note in Fig. 3 d–f that a more coherent center of maximum or minimum convective rainfall anomalies exists in the northern PRD, while the positive or negative anomalies of lightning flash densities do not exhibit such a distinct configuration in Fig. 3a–c. This is because the spatial resolution (2.5° × 2.5°) of the lightning flash rate data is too coarse to discern more detailed information. If higher-resolution gridded lightning flash products were directly available, a maximum or minimum lightning density center would be found at the same location (northern PRD) as anomalous convective rainfall. Actually, this feature can be indirectly verified or partly supported by Zheng et al. (2016), who utilized the relatively higher-resolution lightning data observed from the ground-based lightning detection sensors in Guangdong province to examine the climatology of lightning activity over South China for the period 2001–2012. Note in their Fig. 1a that a remarkable area with maximum densities of climatological total lightning is indeed located around the northern PRD centered on Guangzhou City. Since the center of maximum interannual standard deviations in both the spring convective rainfall and lightning density tends to coincide with that of their climatological maxima due to low-level southerly airflow convergence toward a bell-mouth shaped topography in the northern part of the PRD, the maximum or minimum lightning density center at the northern PRD similar to that in Fig. 3d–f is surely included in Fig. 3a–c. This issue will be further explored when higher-resolution ground-based and/or satellite-based lightning products are available. The spatial differences in the magnitude of composite anomalies associated with frequent and infrequent SCLA years can be clarified by the area-averaged anomaly values over SC of the three variables (Table 2). Note that although the anomaly values are all slightly larger in magnitude in the frequent SCLA years than those in the infrequent SCLA

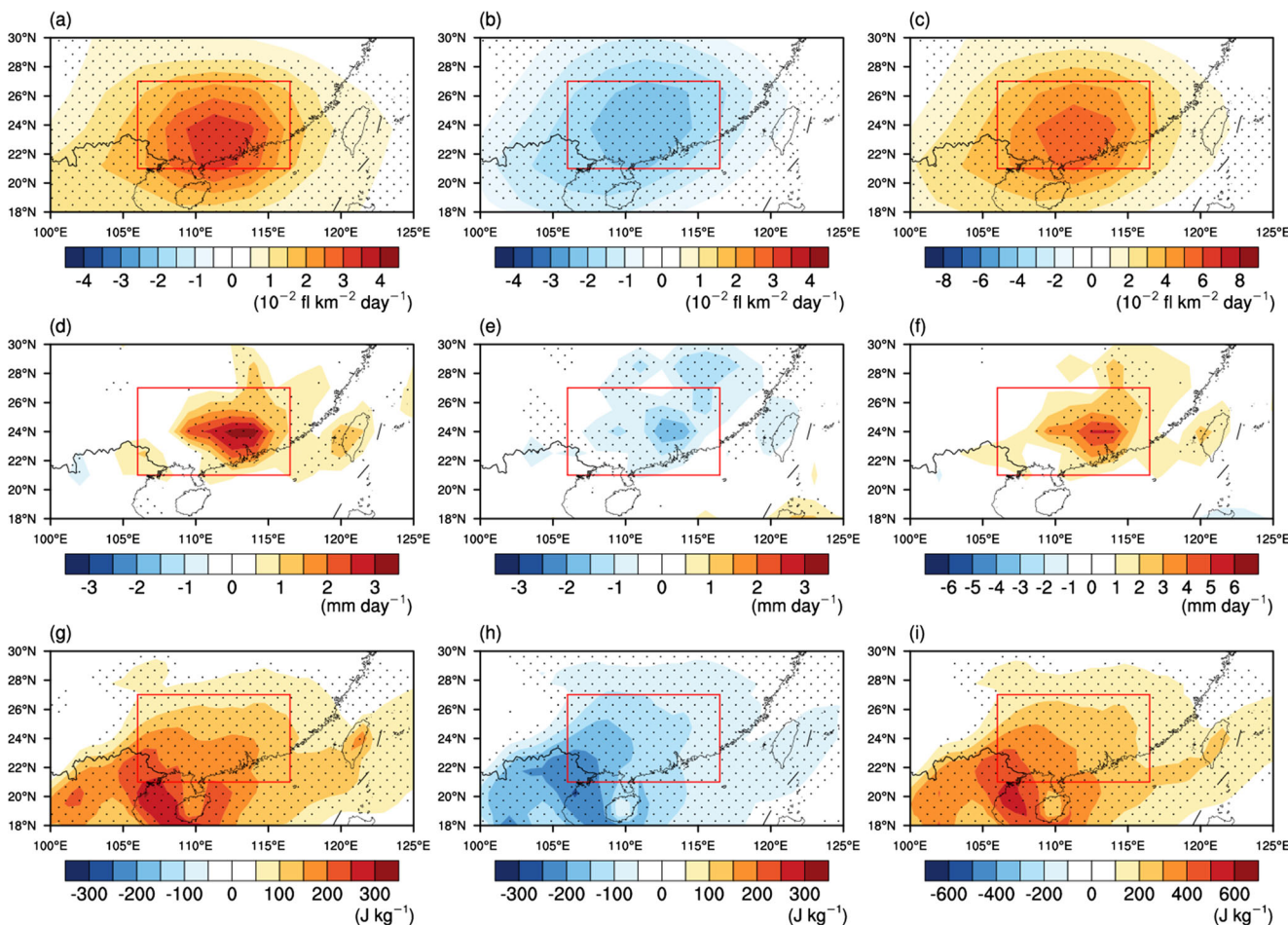


**Fig. 3** Composite anomalies (shading) of spring (March–May) lightning flash rate (FR;  $10^{-2}$  fl  $\text{km}^{-2}$   $\text{day}^{-1}$ ) for **a** the frequent and **b** infrequent SCLA years. **c** Composite differences (shading) between **a** and **b**. **d–f** As in **a–c** but for convective rainfall rate (ConvR,  $\text{mm day}^{-1}$ ). **g–i** As in **a–c**

but for convective available potential energy (CAPE;  $\text{J kg}^{-1}$ ). Stippling indicates the anomalies statistically significant at the 90% confidence level. Red rectangle indicates the key region over South China ( $21^{\circ}$ – $27^{\circ}$  N,  $106^{\circ}$ – $116.5^{\circ}$  E)

years, the sensitivity of lightning activity and convective rainfall to changes in CAPE is identical according to Table 2, with the ratio of lightning density to CAPE anomalies being  $2.0 \times 10^{-4}$  fl  $\text{km}^{-2}$   $\text{day}^{-1}$   $\text{kg J}^{-1}$ , and the ratio of convective rainfall to CAPE anomalies being  $0.64 \times 10^{-2}$   $\text{mm day}^{-1}$   $\text{kg J}^{-1}$ . These results not only illustrate that the interannual variations in SCLA and convective rainfall are consistent and in-phase with those of CAPE but also validate quantitatively the close dependence of SCLA and convective rainfall on CAPE changes.

### 3.3 Physical mechanism for SCLA interannual variability

The spring SCLA anomaly is positively correlated with the ONI in the preceding winter, with a correlation coefficient of 0.51 that is statistically significant at the 95% confidence level (Table 1). The same coefficient is obtained for correlations of each of the spring convective rainfall and CAPE with winter-time ONI (Table 1). To confirm the linkage with ENSO, the

**Table 2** Area-averaged composite anomalies and differences over the SC key region ( $21^{\circ}$ – $27^{\circ}$  N,  $106^{\circ}$ – $116.5^{\circ}$  E) of spring lightning flash rate (FR;  $10^{-2}$  fl  $\text{km}^{-2}$   $\text{day}^{-1}$ ), convective rainfall rate (ConvR;  $\text{mm day}^{-1}$ ),

and convective available potential energy (CAPE;  $\text{J kg}^{-1}$ ) for the frequent SCLA years versus the infrequent SCLA years. Note that these anomalies are statistically significant at the 90% confidence level

	Frequent SCLA years	Infrequent SCLA years	Frequent-minus-infrequent SCLA years
FR	1.78	-1.24	3.02
ConvR	0.57	-0.40	0.98
CAPE	0.89	-0.62	1.51



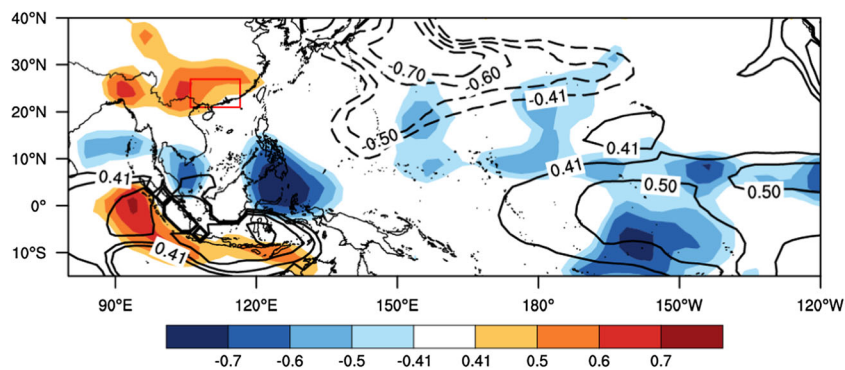


**Fig. 4** Spatial distributions of time-lagged correlation coefficients (contours) between area-averaged spring lightning flash rate anomalies over the SC key region (21°–27° N, 106°–116.5° E) and SSTAs for every grid point during the preceding winter (December–February) and correlation coefficients (shading) between area-averaged winter ONI (5° S–5°

N, 120°–170° W) and subsequent spring lightning flash rate anomalies for every grid point during the period 1998–2014. The correlations are only shown for locations where the coefficients are statistically significant at and above the 95% confidence level. Red rectangle refers to the SC key region

spatial distribution of time-lagged correlations of area-averaged spring SCLA with SSTAs in the preceding winter (December–February) is shown in Fig. 4. Significant positive correlations (>0.41, at the 95% confidence level) are present over the equatorial central eastern Pacific and equatorial Indian Ocean, with significant negative correlations over the extratropical North Pacific. Such a significant correlation pattern is similar to the typical SSTA distribution of an El Niño event. Figure 4 also shows the correlation coefficients between the time series of area-averaged winter ONI and the spring lightning flash rate anomalies for every grid point. Note that the statistically significant positive correlations are indeed concentrated over SC, although the maximum center is located over the western part of the key area. Such a spatial pattern of significant correlations is very similar to that of simultaneous spring correlations between the Nino 3.4 index and lightning flash rates given by Dowdy (2016, see his fig. 1). These results suggest that abnormal SCLA together with convective rainfall and CAPE are strongly associated with ENSO events, with frequent (infrequent) SCLA following El Niño (La Niña) events.

As classified in Section 2.3, the anomalously frequent SCLA years are 1998, 2005, 2012, 2013, and 2014, while the infrequent SCLA years are 1999, 2000, 2008, 2009, and 2011. According to the wintertime ONI value, two of these frequent SCLA years are associated with El Niño events (1997/1998 and 2004/2005), whereas each infrequent SCLA year corresponds to a La Niña event. This indicates an

asymmetric response of anomalous SCLA to warm and cold ENSO events, with a preference for infrequent SCLA to be associated with La Niña conditions. Here, we emphasize the time-lagged impact of the mature ENSO event in wintertime on abnormal SCLA in the following spring; an ENSO event tends to decay during the spring season, but the ENSO-related SST anomaly signals persist for several months, thereby inducing anomalous circulation that affects SCLA (as discussed below). For the above five La Niña events, the wintertime ONI values were all below -0.8 (Table 3), while the ONI values in spring also remained mostly below -0.6 (Table 3), with an exception of spring 2009. With regard to the 2008/2009 La Niña event, though the ONI value increased to -0.2 in spring, positive SST anomalies above 0.5 °C were still present in the western Pacific west of 150° E (not shown), which may have contributed to the formation of local cyclonic circulation over the western North Pacific (see Fig. 5b).

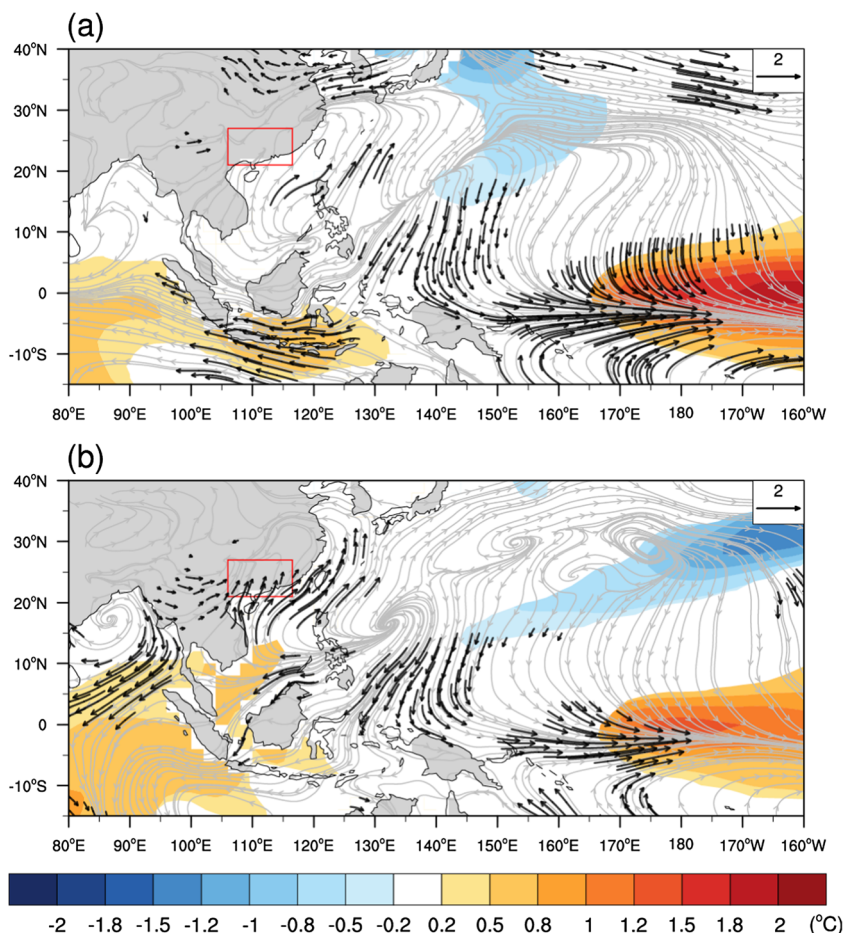
To explore how ENSO-related SSTAs remotely induce anomalous circulation to affect the SCLA, we perform composite analyses to identify the circulation differences. Considering that the anomalies for a variable between anomalously frequent SCLA years and normal years generally tend to have opposite signs to those between anomalously infrequent SCLA years and normal years, the composite frequent-minus-infrequent differences are calculated to simply represent anomalies related to the frequent SCLA years. The inverse can be assumed for the infrequent SCLA cases.

Figure 5 illustrates composite wintertime and springtime SST differences between frequent and infrequent SCLA years. Significant positive SSTAs are found in the central eastern Pacific and the equatorial Indian Ocean (Fig. 5a), with negative SSTAs in the extratropical North Pacific for frequent SCLA years, which is similar to the spatial pattern of significant correlations shown in Fig. 4. Such SSTA distributions are typical features in winter when an El Niño event reaches the mature phase (Wang et al. 2000). As well as significant surface westerlies over the equatorial Pacific and surface

**Table 3** The ONI values (°C) for winter (December–February) and spring (March–May) seasons of five La Niña events associated with infrequent SCLA years

	1999	2000	2008	2009	2011
Winter	-1.5	-1.7	-1.6	-0.8	-1.4
Spring	-1.0	-0.8	-0.9	-0.2	-0.6

**Fig. 5** Composite anomalies between frequent and infrequent SCLA years of SST (shading; °C) and 10-m winds (streamlines and vectors;  $\text{m s}^{-1}$ ) in **a** winter (December–February) and **b** spring (March–May). Only shown are the SST anomalies statistically significant at the 90% confidence level. Statistically significant wind anomalies are shown by black vectors. Red rectangle indicates the key region over South China ( $21^{\circ}$ – $27^{\circ}$  N,  $106^{\circ}$ – $116.5^{\circ}$  E)



easterlies over the Maritime Continent, the atmospheric response of surface winds to tropical positive SSTAs includes an anomalous anticyclone over the western North Pacific (Fig. 5a), with significant southerlies over the South China Sea on the western side of the anticyclone blowing toward SC. Wang et al. (2000) suggested that this anomalous anticyclone is induced both by in situ ocean cooling and subsidence forced remotely by equatorial central eastern Pacific warming. The opposite situations are noted for La Niña events.

In spring when an El Niño event decays, although the positive SSTAs in the equatorial central eastern Pacific weaken noticeably, there are significant positive SSTAs in the southern South China Sea and eastern Bay of Bengal (Fig. 5b). As a result of local and remote responses to the SSTA pattern, statistically significant surface southwesterly anomalies prevail over the South China Sea and converge toward SC (Fig. 5b), forming a large-scale cyclonic circulation favorable for active convection and frequent SCLA over SC. Note that the surface southwesterlies have two sources, one is from the southerly component on the western side of the western North Pacific anticyclone, and the other is from the upstream westerly component over the Indochina Peninsula.

Given that active convection requires stronger updrafts and abundant moisture convergence, Fig. 6 provides composite

differences between frequent and infrequent SCLA years for wind fields at various isobaric surfaces along with vertical motion and water vapor flux. In the upper troposphere (Fig. 6a), there are significant southwesterlies east of  $130^{\circ}$  E, which are part of the anomalous anticyclone that develops in response to positive SSTAs in the central eastern Pacific shown in Fig. 5b. Strong anomalous westerlies prevail over the tropical Indian Ocean, responding to the locally positive SSTAs (Fig. 5b) in conjunction with downstream positive SSTAs in the tropical central eastern Pacific during the decaying phase of a typical El Niño event. Note these westerlies expand northward to  $25^{\circ}$  N and veer northward to form significant southwesterlies over SC (Fig. 6a). The strong southwesterlies produce a divergent environment in the upper troposphere over SC, where the intensity of the abnormal upper-level divergence reaches  $1.5 \times 10^{-6} \text{ s}^{-1}$  (Fig. 6a). This strong dynamical pumping effect is coupled with the low-level convergence caused by anomalous southwesterlies (Figs. 5b and 6c), leading to strong ascending motion in the middle troposphere over SC (Fig. 6b). This enhanced dynamical forcing allows more air parcels to reach their level of free convection, providing a source of lifting, and allowing these parcels to utilize an enhanced thermodynamic environment thereby producing potentially stronger convection and more frequent lightning. Anomalous vertically integrated

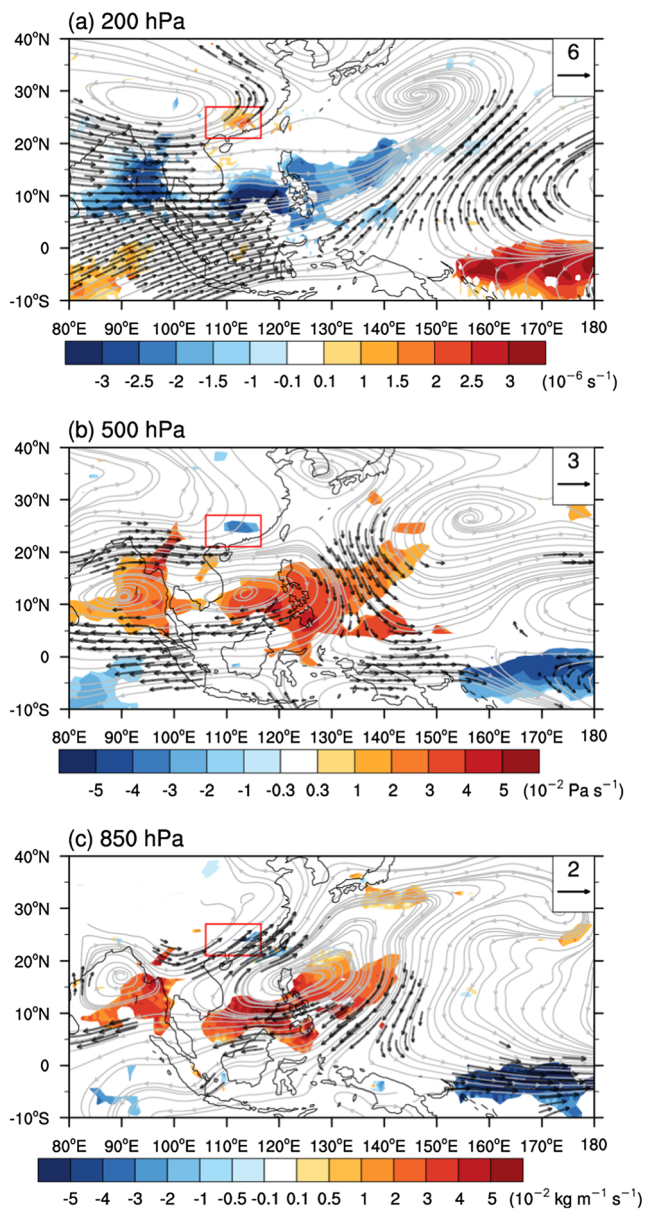


**Fig. 6** Composite anomalies between frequent and infrequent SCLA years of spring (March–May) **a** 200-hPa winds (streamlines and vectors;  $\text{m s}^{-1}$ ) and divergence (shading;  $\text{s}^{-1}$ ), **b** 500-hPa winds (streamlines and vectors;  $\text{m s}^{-1}$ ) and vertical velocity (shading;  $10^{-2} \text{ Pa s}^{-1}$ ), and **c** 850-hPa winds (streamlines and vectors;  $\text{m s}^{-1}$ ) and vertically integrated moisture flux divergence (shading;  $10^{-5} \text{ kg m}^{-1} \text{ s}^{-1}$ ). Only shown are the shaded anomalies statistically significant at the 90% confidence level. The statistically significant wind anomalies are shown by black vectors. Red rectangle indicates the key region over South China ( $21^{\circ}$ – $27^{\circ}$  N,  $106^{\circ}$ – $116.5^{\circ}$  E)

moisture convergence is produced over SC due mostly to low-level southwesterlies transporting water vapor from the South China Sea and northern Bay of Bengal to SC (Fig. 6c). This moisture convergence favors deep convection and resultant frequent SCLA. In contrast, the anomalous circulation forced by La Niña-related SSTA patterns favors abnormal suppressed convection over SC and infrequent SCLA.

### 4 Summary and discussion

In this study, TRMM satellite-estimated convective rain rate and merged LIS/OTD lightning flash rate datasets together with atmospheric ERA-Interim and oceanic ERSST reanalysis products for the TRMM period (1998–2014) have been used to examine the interannual variability in spring lightning activity over SC in relation to ENSO events. Climatologically, southwesterly winds prevail in the lower troposphere over SC during spring. These winds favor the formation of synoptic-scale quasi-stationary frontal systems over SC when they encounter equatorward-intruding cold air, producing strong ascending motion in the middle troposphere and resultant heavy rainfall. Because the lower tropospheric southwesterly winds are also forced by some moderately high topography, especially the Nanling mountains where the wind direction is almost perpendicular to the zonal mountain range, the air parcels are inevitably lifted in mountain regions over the windward side, triggering mesoscale convective systems embedded within the frontal systems, and producing strong thunderstorms accompanied by lightning. Thus, SC has high lightning flash densities (greater than  $2 \times 10^{-2} \text{ fl km}^{-2} \text{ day}^{-1}$ ), with maximum flash densities (even greater than  $5 \times 10^{-2} \text{ fl km}^{-2} \text{ day}^{-1}$ ) concentrated over Guangxi Zhuang Autonomous Region and Guangdong province, decreasing spatially northward toward the Yangtze Basin. Convective rainfall rates have a similar spatial distribution over SC, with maximum rainfall rates exceeding  $3 \text{ mm day}^{-1}$  around the PRD, corresponding well to the maximum lightning flash densities. Larger CAPE in spring of approximately  $300$ – $400 \text{ J kg}^{-1}$  corresponding to the atmospheric instability required for the formation of thunderstorms also shows a northward decreasing spatial distribution similar to that of lightning flash densities over SC, indicating that the larger lightning densities and convective rainfall rates are associated with larger CAPE over SC during spring.

The spring SCLA has a strong year-to-year variability, with larger interannual standard deviation for the period 1998–2014 of the spring-averaged lightning flash rates mostly exceeding  $1.0 \times 10^{-2} \text{ fl km}^{-2} \text{ day}^{-1}$  in magnitude over SC. The standard deviation of the lightning flash rates is characterized by a spatially coherent annular distribution, with maxima greater than  $3.0 \times 10^{-2} \text{ fl km}^{-2} \text{ day}^{-1}$  concentrated around the PRD. Both convective rainfall rates and CAPE also have considerable interannual variability, with their standard deviations exhibiting similar spatial distributions to that of lightning flash rates. Composite anomalies of lightning flash rate, convective rainfall rate, and CAPE for the frequent versus infrequent SCLA years confirm spatially coherent distributions similar to their standard deviations over SC. The area-averaged SCLA exhibits a highly significant correlation with both convective rainfall and CAPE anomalies, indicating that the interannual variations in SCLA are consistent and in-phase with those of CAPE and convective rainfall, because the

CAPE-related thermodynamic environment appears to play a significant role in producing deep convection and consequent lightning over SC.

Importantly, the interannual variability of spring SCLA exhibits a statistically significant correlation with ENSO events, with infrequent SCLA preferentially following La Niña events. Composite differences between anomalously frequent and infrequent SCLA years demonstrate that in spring when an El Niño event decays, significant positive SSTAs persist in the central eastern Pacific and in the equatorial Indian Ocean, with negative SSTAs in the extratropical North Pacific for frequent SCLA years. Moreover, pronounced positive SSTAs occur in the southern South China Sea. The atmospheric local and remote responses of surface winds to the El Niño-related SSTA pattern lead to significant anomalous surface southwesterlies over the South China Sea converging over SC, forming a large-scale cyclonic circulation favorable for active convection and frequent SCLA.

The atmospheric response to the El Niño-related SSTA pattern includes significant westerlies in the upper troposphere over the tropical Indian Ocean, associated with the locally positive SSTAs together with downstream positive SSTA in the tropical central eastern Pacific during the decaying phase. The westerlies expand northward to 25° N and back northward to form significant southwesterlies over SC, producing a divergent environment in the upper troposphere. The strong upper-level divergence is coupled via dynamical pumping with low-level convergent southwesterlies, leading to strong updrafts in the middle troposphere over SC. Such enhanced dynamical forcing lifts more air parcels to reach their level of free convection, allowing these parcels to utilize an enhanced thermodynamic environment thereby producing potentially stronger convection and more frequent lightning. Anomalous moisture convergence is produced over SC mostly by anomalous low-level southwesterlies transporting water vapor from the South China Sea and northern Bay of Bengal to SC, favoring active convection and frequent SCLA. In contrast, the anomalous circulation forced by La Niña-related SSTA patterns leads to anomalously suppressed convection over SC and infrequent SCLA.

It should be mentioned that in the present study, though the positive correlation between the SCLA anomalies and ENSO events is derived from currently available datasets for a still relatively short period (1998–2014), with some exceptions to this relationship, the statistical significance of the relationship has passed the 95% confidence level. Therefore, this statistical relationship substantiates that ENSO is a primary driving force for interannual lightning variability over SC, supporting previous case studies such as Yoshida et al. (2007) and Yuan et al. (2016). In addition, an asymmetric impact of ENSO events on SCLA anomalies may exist in this SCLA–ENSO relationship, in which the infrequent SCLA in spring is often preceded by a La Niña event, but frequent SCLA is not always

preceded by an El Niño event. As shown in Fig. 2, for example, the 2002/2003 and 2006/2007 El Niño events did not result in frequent SCLA, which may be due to cold SSTAs in the western tropical Indian Ocean, as suggested by Chen et al. (2014) and Liu et al. (2018). Note that the SCLA–ENSO relationship may also be dominated by the contributions of a few strong ENSO events, particularly for El Niño events. For instance, the wintertime ONI values of the 1997/1998 super El Niño event were greater than 2 °C as shown in Fig. 2, corresponding to a larger amplitude of abnormal SCLA, thus producing a larger covariance contributing to the correlation coefficient, as suggested by Dowdy (2016). An apparent exception is noted to occur in the 2005/2006 La Niña event, without evident changes in SCLA, which may be due to a modification of the ENSO-induced western North Pacific subtropical anticyclone by the mid-latitude North Pacific SSTA-forced anomalous circulation, as suggested by Wu and Mao (2016). However, the 2012/2013 and 2013/2014 neutral events are followed by anomalously frequent SCLA. These exceptions imply that other factors may play a more important role than El Niño events in generating frequent SCLA. These issues will be explored in the future.

**Acknowledgements** Lightning flash rate data are from the NASA Global Hydrology Resource Center (GHRC) website (<https://ghrc.nsstc.nasa.gov/hydro/?q=LRMTS>). TRMM-estimated convective rainfall along with total rainfall were derived from [https://disc.gsfc.nasa.gov/datasets/TRMM\\_3A25\\_V7/summary?keywords=3A25](https://disc.gsfc.nasa.gov/datasets/TRMM_3A25_V7/summary?keywords=3A25). The atmospheric circulation variables and CAPE were obtained from the ERA-Interim dataset (<https://www.ecmwf.int/en/forecasts/datasets/browse-reanalysis-datasets>). The Extended Reconstructed SST (ERSST) data are available at <https://www1.ncdc.noaa.gov/pub/data/cmb/ersst/v5/netcdf/>, with the Niño 3.4 index calculated from the ERSST dataset from the NOAA website ([https://origin.cpc.ncep.noaa.gov/products/analysis\\_monitoring/ensostuff/ONI\\_v5.php](https://origin.cpc.ncep.noaa.gov/products/analysis_monitoring/ensostuff/ONI_v5.php)). This research was jointly supported by the Strategic Priority Research Program of the Chinese Academy of Sciences (Grant No. XDB40000000), the SOA Program on Global Change and Air–Sea Interactions (Grant No. GAS-IPOVAI-03), and the Natural Science Foundation of China (Grant Nos. 41876020 and 41730963).

## References

- Berrisford P, Dee DP, Fielding K, Fuentes M, Kallberg P, Kobayashi S, Uppala SM (2009) The ERA-Interim Archive, ERA Report Series, No. 1. ECMWF, Reading
- Blakeslee RJ, Mach DM, Bateman MG, Bailey JC (2014) Seasonal variations in the lightning diurnal cycle and implications for the global electric circuit. *Atmos Res* 135–136:228–243. <https://doi.org/10.1016/j.atmosres.2012.09.023>
- Cecil DJ, Buechler DE, Blakeslee RJ (2014) Gridded lightning climatology from TRMM-LIS and OTD: dataset description. *Atmos Res* 135–136:404–414. <https://doi.org/10.1016/j.atmosres.2012.06.028>
- Cecil DJ, Buechler DE, Blakeslee RJ (2015) TRMM LIS climatology of thunderstorm occurrence and conditional lightning flash rates. *J Clim* 28:6536–6547

- Chen J, Wen Z, Wu R, Chen Z, Zhao P (2014) Interdecadal changes in the relationship between Southern China winter-spring precipitation and ENSO. *Clim Dyn* 43:1327–1338
- Christian HJ, Blakeslee RJ, Boccippio DJ et al (2003) Global frequency and distribution of lightning as cd from space by the Optical Transient Detector. *J Geophys Res* 108(D1):4005. <https://doi.org/10.1029/2002JD002347>
- Chronis TG, Goodman SJ, Cecil DJ, Buechler D, Robertson FJ, Pittman J, Blakeslee RJ (2008) Global lightning activity from the ENSO perspective. *Geophys Res Lett* 35:L19804. <https://doi.org/10.1029/2008GL034321>
- Dai J, Wang Y, Chen L, Tao L, Gu J, Wang J, Xu X, Lin H, Gu Y (2009) A comparison of lightning activity and convective indices over some monsoon-prone areas of China. *Atmos Res* 91:438–452
- Dee DP, Uppala SM, Simmons AJ, Berrisford P, Poli P, Kobayashi S, Andrae U, Balmaseda MA, Balsamo G, Bauer P, Bechtold P, Beljaars ACM, van de Berg L, Bidlot J, Bormann N, Delsol C, Dragani R, Fuentes M, Geer AJ, Haimberger L, Healy SB, Hersbach H, Hólm EV, Isaksen I, Kållberg P, Köhler M, Matricardi M, McNally AP, Monge-Sanz BM, Morcrette JJ, Park BK, Peubey C, de Rosnay P, Tavolato C, Thépaut JN, Vitart F (2011) The ERA-interim reanalysis: configuration and performance of the data assimilation system. *Q J R Meteorol Soc* 137:553–597. <https://doi.org/10.1002/qj.828>
- Dowdy AJ (2016) Seasonal forecasting of lightning and thunderstorm activity in tropical and temperate regions of the world. *Sci Rep* 6: 20874. <https://doi.org/10.1038/srep20874>
- Dowdy AJ, Mills GA (2012) Characteristics of lightning-attributed fires in south-east Australia. *Int J Wildland Fire* 21:521–524
- Feng J, Li J (2011) Influence of El Niño Modoki on spring rainfall over South China. *J Geophys Res* 116:D13102. <https://doi.org/10.1029/2010JD015160>
- Goodman SJ, Buechler DE, Knupp K, Driscoll D, McCaul Jr EE (2000) The 1997–98 El Niño event and related wintertime lightning variations in the southeastern United States. *Geophys Res Lett* 27:541–544
- Holle RL (2008) Annual rates of lightning fatalities by country. 2nd international lightning meteorology conference, Tuscon, Arizona
- Huang B, Thorne PW, Banzon VF, Boyer T, Chepurin G, Lawrimore JH, Menne MJ, Smith TM, Vose RS, Zhang HM (2017) Extended re-constructed sea surface temperature, version 5 (ERSSTv5): upgrades, validations, and intercomparisons. *J Clim* 30:8179–8205
- Li J, Mao J (2019) Factors controlling the interannual variation of 30–60-day boreal summer intraseasonal oscillation over the Asian summer monsoon region. *Clim Dyn* 52:1651–1672
- Li W, Wang D, Lei T, Wang H (2009) Convective and stratiform rainfall and heating associated with the summer monsoon over the South China Sea based on TRMM data. *Theor Appl Climatol* 95:157–163
- LinHo LH, Huang XL, Lau NC (2008) Winter-to-spring transition in East Asia: a planetary-scale perspective of the South China spring rain onset. *J Clim* 21:3081–3096
- Liu B, Zhu C, Su J, Hua L, Duan Y (2018) Why was the western Pacific subtropical anticyclone weaker in late summer after the 2015/2016 super El Niño? *Int J Climatol* 38:55–65
- Monkam D (2002) Convective available potential energy (CAPE) in northern Africa and tropical Atlantic and study of its connections with rainfall in central and West Africa during summer 1985. *Atmos Res* 62:125–147
- Petersen WA, Nesbitt SW, Blakeslee RJ, Cifelli R, Hein P, Rutledge SA (2002) TRMM observations of intraseasonal variability in convective regimes over the Amazon. *J Clim* 15:1278–1294
- Pokhrel S, Sikka DR (2013) Variability of the TRMM-PR total and convective and stratiform rain fractions over the Indian region during the summer monsoon. *Clim Dyn* 41:21–44
- Ramesh Kumar P, Kamra AK (2012) The spatiotemporal variability of lightning activity in the Himalayan foothills. *J Geophys Res* 117: D24201. <https://doi.org/10.1029/2012JD018246>
- Saha U, Singh D, Midya SK, Singh RP, Singh AK, Kumar S (2017) Spatio-temporal variability of lightning and convective activity over south/South-East Asia with an emphasis during El Niño and La Niña. *Atmos Res* 197:150–166. <https://doi.org/10.1016/j.atmosres.2017.07.005>
- Tao SY, Chen LX (1987) A review of recent research on the east Asian monsoon in China. In: Chang CP, Krishnamurti TN (eds) *Monsoon Meteorology*. Oxford University Press, Oxford, pp 60–92
- Trapp RJ, Diffenbaugh NS, Brooks HE, Baldwin ME, Robinson ED, Pal JS (2007) Changes in severe thunderstorm environment frequency during the 21st century caused by anthropogenically enhanced global radiative forcing. *Proc Natl Acad Sci* 104:19719–19723
- Wan R, Wu G (2007) Mechanism of the spring persistent rains over southeastern China. *Sci China Ser D-Earth Sci* 50(1):130–144
- Wang B, Wu R, Fu X (2000) Pacific-east Asian teleconnection: how does ENSO affect east Asian climate? *J Clim* 13:1517–1536
- Williams ER (1995) Meteorological aspects of thunderstorms. In: *Handbook of Atmospheric Electrodynamics*. CRC Press, Boca Raton, Florida, pp. 27–60
- Williams E, Renno N (1993) An analysis of the conditional instability of the tropical atmosphere. *Mon Wea Rev* 121:21–36
- Williams E, Rothkin K, Stevenson D (2000) Global lightning variations caused by changes in thunderstorm flash rate and by changes in the number of thunderstorms. *J Appl Meteorol* 39:2223–2230
- Wu X, Mao J (2016) Interdecadal modulation of ENSO-related spring rainfall over South China by the Pacific decadal oscillation. *Clim Dyn* 47:3203–3220
- Wu X, Mao J (2018) Spatial and interannual variations of spring rainfall over eastern China in association with PDO-ENSO events. *Theor Appl Climatol* 134:935–953
- Xu W, Zipser EJ, Liu C (2009) Rainfall characteristics and convective properties of Mei-Yu precipitation systems over South China and Taiwan, part I: TRMM observations. *Mon Wea Rev* 137:4261–4275
- Xu W, Zipser EJ, Liu C, Jiang H (2010) On the relationships between lightning frequency and thundercloud parameters of regional precipitation systems. *J Geophys Res* 115:D12203. <https://doi.org/10.1029/2009JD013385>
- Yoshida S, Morimoto T, Ushio T, Kawasaki Z (2007) ENSO and convective activities in Southeast Asia and western Pacific. *Geophys Res Lett* 34:L21806. <https://doi.org/10.1029/2007GL030758>
- Yuan T, Qie X (2008) Study on lightning activity and precipitation characteristics before and after the onset of the South China Sea summer monsoon. *J Geophys Res* 113:D14101. <https://doi.org/10.1029/2007JD009382>
- Yuan T, Di Y, Qie K (2016) Variability of lightning flash and thunderstorm over east/Southeast Asia on the ENSO time scales. *Atmos Res* 169:377–390
- Zhang W, Meng Q, Ma M, Zhang Y (2011) Lightning casualties and damages in China from 1997 to 2009. *Nat Hazards* 57:465–476
- Zheng D, Zhang Y, Meng Q, Chen L, Dan J (2016) Climatology of lightning activity in South China and its relationship to precipitation and convective available potential energy. *Adv Atmos Sci* 33:365–376
- Zipser EJ, Liu CT, Cecil DJ, Nesbitt SW, Yorty DP (2006) Where are the most intense thunderstorms on earth? *Bull Amer Meteor Soc* 87: 1057–1071